Title

Electrolyte-Dependent Oxygen Evolution Reactions in Alkaline Media: Electrical Double Layer and Interfacial Interactions

Journal

ACS Applied Materials & Interfaces, 11(37)

ISSN

1944-8244

Authors

Li, Guang-Fu
Divinagracia, Maricor
Labata, Marc Francis
et al.

Publication Date

2019-09-18

DOI

10.1021/acsami.9b06889

Peer reviewed

ACS APPLIED MATERIALS & INTERFACES

Research Article

Cite This: ACS Appl. Mater. Interfaces XXXX, XXX, XXX−XXX

www.acsami.org

Electrolyte-Dependent Oxygen Evolution Reactions in Alkaline Media: Electrical Double Layer and Interfacial Interactions

Guang-Fu Li,*[,†] Maricor Divinagracia,[†,§] Marc Francis Labata,[‡] Joey D. Ocon,[§] and Po-Ya Abel Chuang*[,†,‡]

[†]Department of Mechanical Engineering, University of California Merced, California 95343, United States

[‡]Environmental Systems Graduate Program, University of California, Merced 94343, California, United States

[§]Department of Chemical Engineering, College of Engineering, University of the Philippines Diliman, Quezon City 1101, Philippines

Supporting Information

ABSTRACT: Traditional understanding of electrocatalytic reactions generally focuses on either covalent interactions between adsorbates and the reaction interface (i.e., electrical double layer, EDL) or electrostatic interactions between electrolyte ions. Here, our work provides valuable insights into interfacial structure and ionic interactions during alkaline oxygen evolution reaction (OER). The importance of inner-sphere OH^- adsorption is demonstrated as the IrO_x activity in 4.0 M KOH is 6.5 times higher than that in 0.1 M KOH. Adding $NaNO_3$ as a supporting electrolyte, which is found to be inert for long-term stability, complicates the electrocatalytic reaction in a half cell. The nonspecially adsorbed Na^+ in the outer compact interfacial layer is suggested to form a stronger noncovalent interaction with OH^- through hydrogen bond than adsorbed K^+, leading to the decrease of interfacial OH^- mobility. This hypothesis highlights the importance of outer-sphere adsorption for the OER, which is generally recognized as a pure inner-sphere process. Meanwhile, based on our experimental observations, the pseudocapacitive behavior of solid-state redox might be more reliable in quantifying active sites for OER than that measured from the conventional EDL charging capacitive process. The interfacial oxygen transport is observed to improve with increasing electrolyte conductivity, ascribing to the increased accessible active sites. The durability results in a liquid alkaline electrolyzer which shows that adding $NaNO_3$ into KOH solution leads to additional degradation of OER activity and long-term stability. These findings provide an improved understanding of the mechanistic details and structural motifs required for efficient and robust electrocatalysis.

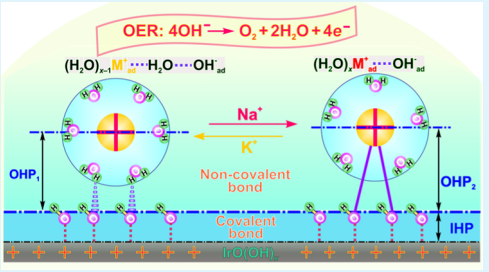

KEYWORDS: *oxygen evolution reaction, oxygen transport, supporting electrolyte, interfacial interactions, electrical double layer*

1. INTRODUCTION

Industrial water splitting typically takes place in a liquid KOH electrolyte because reactions in acidic electrolytes can cause serious corrosion.[1] The efficiency of the water-splitting processes is limited primarily by the oxygen evolution reaction (OER) because of the sluggish kinetics.[2−4] Over the last few decades, a wide range of OER catalysts have been developed, but the activity and stability are still much less than what are required for broad applications. An enhanced understanding of the oxygen evolution process at a fundamental level is important to enable new breakthroughs.

The thin-film rotating disk (TF-RDE) and the thin-film rotating ring disk (TF-RRDE) electrode setups are the most widely used systems to evaluate new electrocatalysts.[5−7] In these systems, the electrolyte solution must be ionically conductive to reduce charge transport resistance. Unfortunately, all alkaline electrolytes have an inherent drawback that the conductivity of OH^- (198 S cm^2 mol^{-1}) is much lower than that of H^+ (350 S cm^2 mol^{-1}).[8] As a result, the alkaline OER is highly sensitive to the electrolyte. Therefore, enhancing the anion mobility in the electrolyte solution has attracted significant research attention. The alkaline electrolyte solutions in TF-RDE/RRDE systems, such as KOH and NaOH, are commonly assumed to be inert spectators with negligible interaction with the studied catalysts. A large variety of electrolytes with various types and concentrations are being considered when investigating catalyst properties.[9,10] Obtaining the intrinsic properties of novel catalysts remains challenging, as OER pathways and mass transport are likely influenced by the applied electrolyte.[9,11−14] It is found that some ions in the electrolyte, such as alkali metal cations, can influence electrochemical activity and stability because of the charge-mediated interplay with the electrode surface.[15−17]

In principle, the alkaline OER is a very complex multistep reaction involving surface-adsorbed intermediates, such as OH_{ad}, O_{ad}, and OOH_{ad}.[4,18] A fundamental understanding of

Received: April 19, 2019
Accepted: August 22, 2019
Published: August 22, 2019

DOI: 10.1021/acsami.9b06889
ACS Appl. Mater. Interfaces XXXX, XXX, XXX−XXX

OER mechanism involves characterization of four electron-transfer steps on active sites, which convert OH^- to O_2 molecules.[11] The favorable properties of electrocatalysts strongly depend on the quality of interactions among all species present at the reaction interface. These interfacial interactions influence reactant adsorption, bond formation, and bond breaking. In the case of aqueous electrolytes, interactions can be generally classified into two categories.[17,19] One is direct bonding between adsorbates and catalysts, which involves chemisorption, electron transfer, and release of ion hydration shell. The other interaction is formed by weak electrostatic forces, which depends on the ions in the reaction interface. The range of electrochemical behaviors associated with these two bonds is broad. However, the origin of the observed sensitivity of charge transfer to interfacial structure remains elusive. This is mainly because the effects of noncovalent interactions are often ignored when analyzing electrocatalytic OER. Noncovalent interactions, such as hydrogen bonding, cation−OH^- bonding, and cation−water bonding, can affect the adsorbate states, leading to the variation in the electron-transfer rate.[17]

During the OER processes, the layered structure of adsorbates at the catalyst/electrolyte interface forms a hydrous electrical double layer (EDL).[3,20−23] Identifying the reaction interface provides new insights into high-efficiency OER but poses a technical challenge because of the lack of in situ characterization tools.[21−23] The adsorbed ions in the EDL form a potential gradient across a few hundred angstroms, which determines the reaction rate.[24−26] During the electron-transfer reaction, the continuous reconstruction of EDL makes it more difficult to investigate the EDL structure and behaviors directly.[21,23,27] During OER, fast reactant supply and product removal are required to achieve high reaction rates.[14] For instance, the generated O_2 should be quickly removed from the EDL to avoid blocking the active sites. In general, migration is caused by electric charge and its effect can be neglected for the electrically neutral O_2 species. Thus, interfacial O_2 transport is mainly driven by diffusion and convection forces.[6] Using the RDE/RRDE apparatus, the effect of convection can be controlled accurately by setting the electrode rotating rate. In this context, the interfacial oxygen transport can be studied experimentally.

The charge and mass transport resistances in OER processes can be minimized by well-designed electrochemical systems and measurement methods. The electrolyte, acting as a key component in the electrochemical systems, is responsible for conducting reactants and products and thus drives the associated electron-charge-transfer reaction.[8] The nature of the electrolyte solution, for example, ion types and concentration, affects charge migration and mass diffusion in the reaction interface, determining the EDL microstructure and behaviors.[28−30] Aqueous inert or inactive salt is primarily employed as the supporting electrolyte for charge conductors.[25] Adding excess supporting electrolyte can suppress the potential gradient in EDL and reduce the ion migration of electroactive species in the electric field.[25,31] However, it is still uncertain whether the extraneous cations or anions in the supporting electrolyte would impact on electrocatalytic OER, and if so by how much.

Here, we report the effect of electrolyte concentration and composition on the activity and stability of electrocatalyzing OER in alkaline media. The covalent and noncovalent interactions coexisted in the EDL are responsible for such effect. When adding the support electrolyte $NaNO_3$ into the KOH solution, it is demonstrated that the interfacial inner-sphere behaviors, such as the special adsorption of OH^- and O_2 transport in EDL, are crucial for the high-efficiency OER. However, the cation interactions through an outer-sphere mechanism, which have not been reported previously, have a strong impact on adsorbed OH^--activity and in turn on OER. This phenomenon confirms that the inner-sphere model has a limited function to describe the overall OER process.

2. EXPERIMENTAL SECTION

2.1. Preparation of a Thin-Film Catalyst Layer. Prior to depositing a catalyst layer (CL) on the RDE/RRDE disk electrode, a uniform catalyst ink typically composed by 5 mg of IrO_x catalyst, 54 μL of Nafion ionomer solution (5 wt %), and 4 mL of anhydrous ethanol was prepared by an ultrasonic dispersion method. The disk electrode made of glassy carbon was polished with a 50 nm Al_2O_3 suspension and cleaned with water. The resulting ink was then drop-cast onto the entire surface of the clean disk electrode by a 2−20 mL adjustable micropipette and dried under a 600 W infrared lamp. The targeted loading of each sample was 0.24 mg cm^{-2}.

2.2. Electrochemical Measurements of TF-RDE/RRDE. Alkaline electrolyte solutions with various concentrations and compositions were prepared and studied for electrocatalytic OER. One batch of experiments used were performed with KOH solutions ranged from 0.1 to 4.0 M and the other batch was performed with KOH + $NaNO_3$-mixed solutions having a constant concentration of total cation/anion ions at 3.0 M. N_2 was purged into the electrolyte solution throughout the experimental process, except for the stability assessment where O_2 was used. Classic electrochemical techniques, such as cyclic voltammetry (CV), linear sweep voltammetry (LSV), and electrochemical impedance spectroscopy (EIS), were performed to characterize the electrolyte effects. CV curves were obtained under static conditions; while LSV and EIS processes involved the electrode rotation at a speed of 1600 rpm in order to facilitate mass transport and interfacial O_2 removal. The collected Nyquist impedance diagrams from 100 kHz to 0.1 Hz were simulated by a build-in CHI program. For stability evaluation, 10 000 potential cycles from 0.8 to 1.0 V were performed at a scan rate of 100 mV s^{-1} under the O_2-purged condition.

The RRDE setup consists of two electrodes, that is, an inner glass carbon disk electrode and an outer Pt-ring electrode. A CHI 750E bipotentiostat was used to measure the bichannel electrochemical reaction rates. Staircase voltammetry (SCV) with a step period of 10 s was carried out on the disk electrode, where EDL charging current can be minimized. The Pt-ring potential was set to 0.4 V so that the oxygen transported from the disk could be reduced rapidly. To avoid using the pH-dependent potential, all potentials (E_{RHE}) reported in this work were converted to the reversible hydrogen electrode (RHE) by the following equation

$$E_{RHE} = E_{RE} + 0.059pH + E_{o,RE} \quad (1)$$

where E_{RE} is the experimental potential measured against the applied Hg/HgO reference electrode. The standard potential of the reference electrode ($E_{o,RE}$) is measured to be 0.081 V in 1.0 M KOH electrolyte as previously reported.[20]

2.3. Durability Tests in a Liquid Alkaline Electrolyzer. Durability tests were carried out in a traditional alkaline electrolyzer, including an OER working electrode (WE) and a Pt gauze counter electrode (CE). To prepare the WE, catalyst ink mixed with IrO_x and Nafion ionomer was sonicated for 30 min. The weight ratio of IrO_x to ionomer was set to be 1/2 for achieving optimal activity and stability based on our previous work.[32] The dispersed ink was then drop-cast on a carbon fiber paper with a microporous layer (MPL) to form a gas diffusion electrode (GDE). The fabricated GDE was dried under an infrared lamp and subsequently cut into 1.5 × 1.5 cm^2 active area. The catalyst loading we loaded was 3.0 mg cm^{-2}. Durability tests were

DOI: 10.1021/acsami.9b06889
ACS Appl. Mater. Interfaces XXXX, XXX, XXX−XXX

conducted in a constant current mode of 50 mA cm^{-2} at room temperature.

2.4. Physicochemical Characterization. The pH value of each studied electrolyte solution was measured by Mettler Toledo S220. The pH probe was Max Pro-ISM from Mettler Toledo, which provides high accuracy in alkaline environment. The pH probe was calibrated by three standard buffer solutions (pH = 4.01, 7.0, and 10.0). The mean particle size and ionic conductivity of electrolyte solutions were measured by Malvern Zetasizer Nano ZS90. The ink solution was sonicated for 30 min and then filled in a quartz cell for ZS90 measurement.

The scanning electron microscopy (SEM) images of GDE were taken by Zeiss Field Emission GeminiSEM 500 at 5 kV. X-ray diffraction (XRD) patterns were obtained using a PANalytical X'Pert PRO with a Co radiation (λ = 1.7902 Å) at 40 kV and 45 mA.

3. RESULTS AND DISCUSSION

3.1. Illustration of Electrolyte-Dependent EDL and Interactions during OER. In this work, we selected widely used commercial Ir oxide (IrO_x) as the OER catalyst. IrO_x, which has an amorphous structure and 32.5 m^2 g^{-1} Brunauer–Emmett–Teller surface area, exhibits outstanding activity and stability in alkaline media as reported in our previous work.[20,23] Nafion ionomer was used as a stabilizing and binding agent in the CL. The weight ratio of Nafion ionomer to IrO_x catalyst is 1/2 to ensure a stable and high-efficiency OER.[32] To enable OER processes, the hydrated IrO_x initially experiences a phase transition to form a hydrophilic three-dimensional hydroxylated shell consisted of $IrO(OH)_x$.[33,34] Dissimilar mechanisms of electron-transfer reactions might occur in different electrolyte solutions. The electrolytes within the TF-RDE/RRDE system provide abundant OH^-, water, ions, and a buffer region to keep the local pH and ionic strength on the interface stable during OER.[11]

The overall electrocatalytic OER on Nafion–IrO_x is widely accepted as a $4e^-$ transfer process that involves several intermediates and elementary reaction steps.[11,29,35] Depending on the nature of the applied electrolytes, such as concentration and type, the hydrated EDL is formed between the CL surface and the adjacent aqueous electrolyte. Given that the concentration of the electrolyte is usually ≥0.1 M, the impact of diffuse layers can be ignored.[36] As illustrated in Figure 1, the

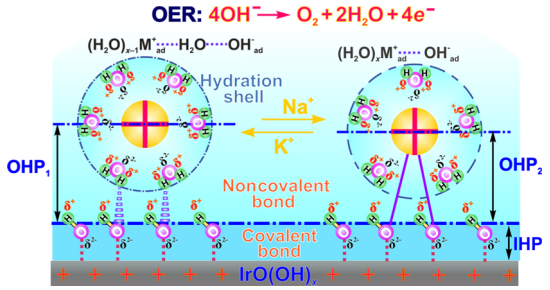

Figure 1. Schematic illustration of the proposed interfacial interaction between the adsorbed OH_{ad}^- and the alkali metal cation (M_{ad}^+).

ions are transported and adsorbed in the EDL during electrochemical processes. The reactant OH^- ions diffuse and migrate into the inner Helmholtz plane (IHP) of EDL in the presence of diffusion and electric forces, that is, $OH_{ad}^- \rightarrow OH_{ad} + e^-$.[17,23,36] The IHP consists of chemisorbed O_2, specially adsorbed OH_{ad}^- and solvent H_2O. The solvated alkaline metal cation, M_{ad}^+ (such as Na^+/K^+), can only be nonspecially absorbed at an outer Helmholtz plane (OHP) to balance the charge in EDL. The solvated molecular O_2 (diffused from IHP) and M_{ad}^+ thus populate the OHP. The interaction between M_{ad}^+ and the charged electrode surface involves only long-range electrostatic forces, which are widely accepted to be independent of the cations and electrode properties.[25]

The deprotonation of OH_{ad} intermediate by transferring proton to OH_{ad}^- can only occur at IHP followed by the first electron transfer from OH_{ad}^- to OH_{ad}. As a result, a stable H_2O molecule and active O_{ad} are generated. In this context, the OER is typically classified as an inner-sphere reaction where the electron transfer takes place only at IHP.[17,36] This concept implies that the OER is highly sensitive to the specially adsorbed OH_{ad}^- from the bulk electrolyte. Nevertheless, using the inner-sphere mechanism cannot illustrate the effect of surface-independent outer-sphere adsorbates on the overall rate of electrocatalytic reaction.[37,38] The effective OH_{ad}^- activity in IHP might be different from that in the bulk electrolyte because of complicated interactions between different species throughout the electrochemical processes. For instance, OH_{ad}^- can form direct chemical bonds with the hydroxylated Ir-based interface, leading to a higher ionic concentration than that through electrostatic interaction in EDL.[39] In the presence of the supporting electrolyte, it is possible that the extraneous anions and cations attracted in EDL are more than inert spectators in the electrocatalytic reaction. The nonspecifically adsorbed M_{ad}^+ ions are stable at OHP through a noncovalent (or ionic) bond with OH_{ad}^-. These cations are highly solvated and are classically represented as a cluster $(H_2O)_xM_{ad}^+$. Depending on the properties of the cations, this noncovalent bonding causes the formation of $(H_2O)_xM_{ad}^+\square\square\square OH_{ad}^-$ (corresponding to the direct ion–dipole interactions between the cation and adsorbed OH_{ad}^- species) or $(H_2O)_{x-1}M_{ad}^+\square\square\square H_2O\square\square\square$-$OH_{ad}^-$ clusters (corresponding to the hydrogen bonding between hydrated water and adsorbed OH_{ad}^-).[17] As shown in Figure 1, the former is likely to reduce OH_{ad}^- activity in IHP owing to direct $M-OH_{ad}^-$ bonding. In the latter case, the bridge-type interaction of OH_{ad}^- and M_{ad}^+ has a negligible effect on the OH_{ad}^- activity because of an extra H_2O buffer layer. This proposed bonding model is different from the classic outer-sphere reaction, reported by Strmcnik et al.[17] and Huang and Nagy,[40] where OH_{ad}^- anions only serve as a bridge that anchors the hydrated cation at OHP. Here, OH_{ad}^- located in IHP is also the reactive species during the EDL charging process and electron-transfer reactions. The noncovalent bonding strength between OH_{ad}^- and M_{ad}^+ determines OH_{ad}^- mobility in the IHP, which might affect electrocatalytic OER.

Oxygen evolution involves transformation from adsorbed species to highly concentrated oxygen gas phase following the four processes: nucleation, growth, detachment, and transport of bubbles.[41] The CL in TF-RDE/RRDE is immersed in aqueous electrolyte solution throughout electrochemical measurements. The electrolyte solution might affect the molecular O_2 formation and transport from IHP to bulk because of the change of EDL structure.

3.2. Physicochemical Properties of Electrolyte Solution. The KOH concentration studied in this work ranges from 0.1 to 4.0 M, which covers the reported data in most relevant literature.[42−46] When adding the supporting electrolyte $NaNO_3$ to KOH, the total concentration of the mixed electrolytes was kept constant, that is, 3.0 M, to maintain

DOI: 10.1021/acsami.9b06889
ACS Appl. Mater. Interfaces XXXX, XXX, XXX−XXX

identical ionic strength. A higher ionic concentration was not used because of the solubility limitation of the mixed $NaNO_3$ + KOH solutions. On the basis of dynamic light scattering, the measured hydrodynamic size in Figure 2a confirms the formation of an aggregate state in various aqueous electrolytes. In the absence of $NaNO_3$, the average hydrodynamic diameter increases almost linearly with increasing KOH concentration. In contrast, the size in mixed KOH + $NaNO_3$ solutions decreases with KOH concentration, indicating that the addition of $NaNO_3$ promotes the cluster formation.

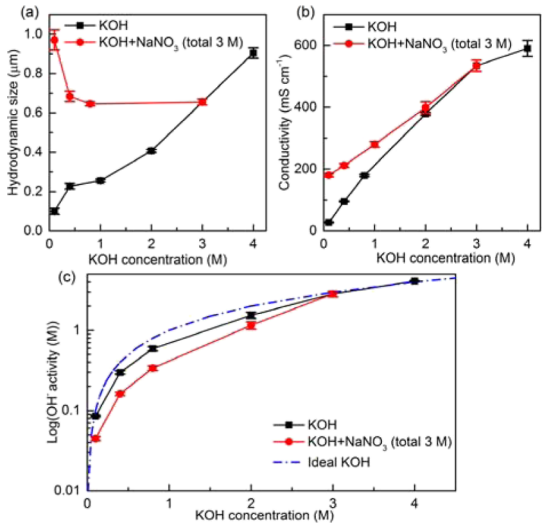

Figure 2. Characterization of electrolyte intrinsic properties as a function of KOH concentration. (a) Hydrodynamic size based on dynamic light scattering, (b) ionic conductivity, and (c) OH^- activity of bulk electrolyte solution.

Figure 2b confirms a strong dependence of ionic conductivity on electrolyte. KOH and $NaNO_3$ are known to be strong electrolytes in water, and the total ionic conductivity increases linearly with the sum of electrolyte concentration. For KOH solution, deviation from linearity can be observed, especially at higher concentrations, which is consistent with the agglomeration behaviors as observed in Figure 2a. Adding $NaNO_3$ improves the ionic conductivity by comparing to a same-concentration KOH solution. However, such improvement is hindered by the large size of the ion clusters and strong electrostatic interactions with KOH. Furthermore, both the conductivity of Na^+ or NO_3^- (refer to Table S1 in the Supporting Information) is much lower than that of K^+ or OH^-. Although with the same total ion concentration, 3.0 M KOH has approximately 3 times higher conductivity than 0.1 M KOH + 2.9 M $NaNO_3$.

In chemistry, pH is commonly used to describe the acidity or basicity of an aqueous solution. In our experiment, a specialized pH sensor with high alkali glass membrane was used to minimize the "alkaline error". The measured results for pure KOH solutions agree well with the ideal values as shown in Figure 2c. The slight deviation, especially at high concentration, is suspected to be due to the enhanced agglomeration of ion clusters. In the mixed solution of KOH + $NaNO_3$, the OH^- activity is significantly lower than that in the same concentration KOH solution. Compared with K^+, Na^+ cations have a smaller ionic radius and can form ionic clusters with negatively charged OH^- more easily (see Table S1 in the Supporting Information).[8] Therefore, the presence of Na^+ reduces OH^- mobility and the corresponding electrolyte pH. In this work, all reported potentials have been adjusted against RHE based on KOH concentration, which allows for direct comparison of catalyst activity while changing the pH.[11]

3.3. Electrocatalytic OER in KOH Electrolytes. In the potential range of 0.4−1.4 V, the CV curves of IrO_x shown in Figure S1 (refer to the Supporting Information) exhibit hybrid capacitive behaviors. The current can be formed by two mechanisms: diffusion-controlled pseudocapacitance (because of solid-state Faradaic redox reaction) and surface-controlled EDL capacitance (because of EDL charging/discharging

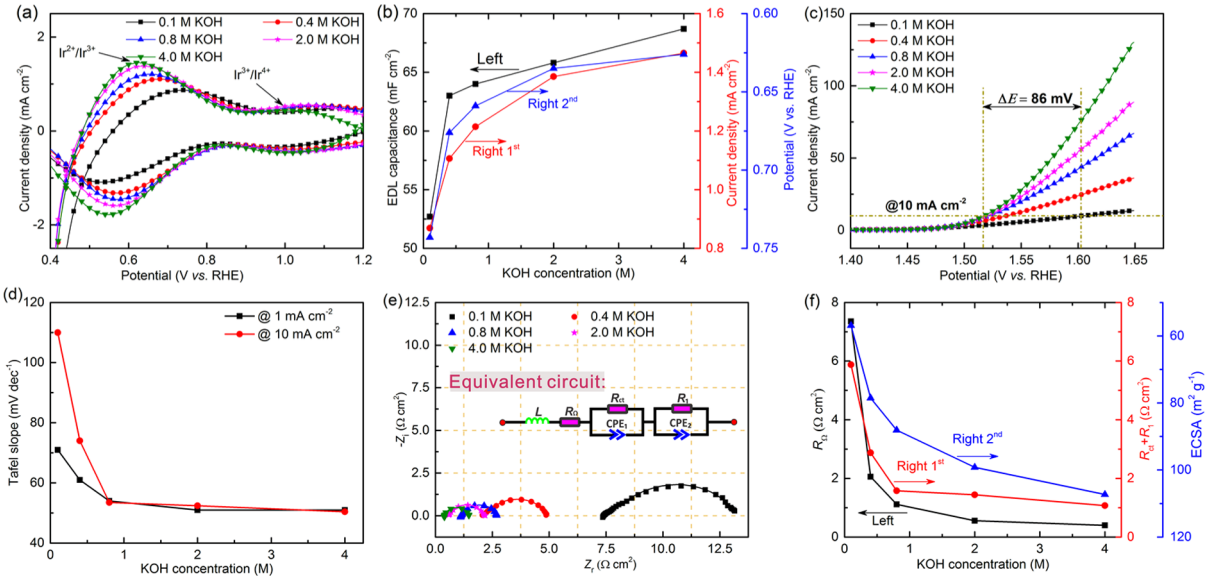

Figure 3. Effects of KOH electrolyte on electrocatalytic OER. (a) Pseudocapacitive behaviors based on CV results at 50 mV s^{-1}, (b) EDL charging capacitance (C_{EDL}), pseudocapacitive current density (j_{ps}), and Ir^{2+}/Ir^{3+} oxidation peak potential, (c) LSV curves at 2 mV s^{-1}, (d) Tafel slopes at 1 and 10 mA cm^{-2}, and (e) EIS spectra at 1.55 V. Symbols—raw data; lines—model prediction. The inset is a simulated equivalent circuit, and (f) R_Ω, R_{ct} + R_1, and ECSA as a function of KOH concentration.

DOI: 10.1021/acsami.9b06889
ACS Appl. Mater. Interfaces XXXX, XXX, XXX−XXX

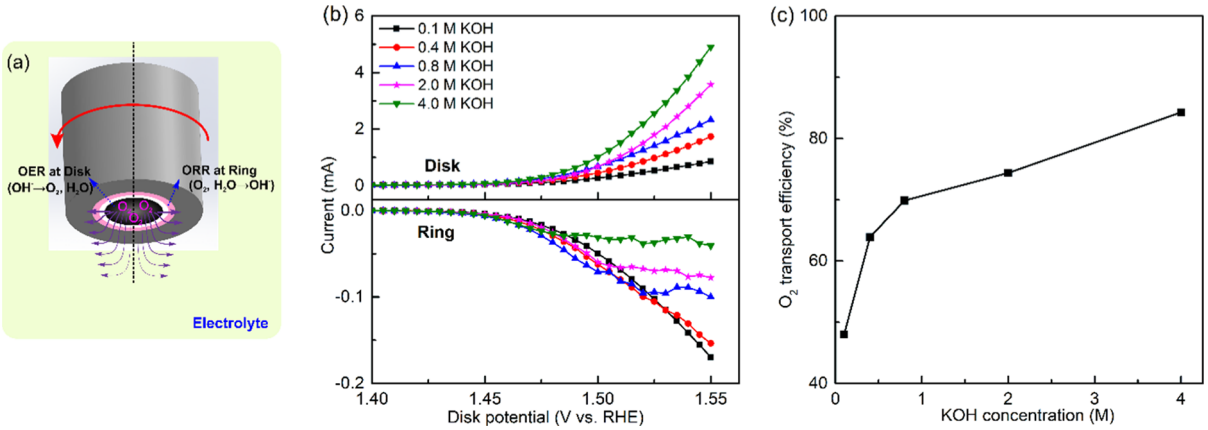

Figure 4. Effect of KOH electrolyte on interfacial O_2 transport. (a) Schematic illustration of O_2 behaviors in the TF-RRDE configuration. (b) SCV curves in RRDE configuration (Pt ring at 0.40 V vs RHE) at a rotating rate of 1600 rpm, and (c) O_2 transport efficiency at 0.5 mA of disk current as a function of KOH concentration.

processes).[8,47] Conventionally, either pseudocapacitive behavior or EDL-capacitive behavior is used to represent the accessible active sites during electron-transfer reactions.[48−50] To demonstrate a pure pseudocapacitive process, the raw CV data are processed by subtracting the EDL charging/discharging current density obtained at the same potential scan rate (50 mV s^{-1}, Figure S2). As shown in Figure 3a, two peaks observed at the low and high potentials are identified as Ir^{2+}/Ir^{3+} and Ir^{3+}/Ir^{4+} redox couples, respectively. Figure 3b quantifies the potential shift of the Ir^{2+}/Ir^{3+} oxidation peak. It is found that increasing the KOH concentration can accelerate the diffusion-controlled redox process, especially when the KOH concentration is below 2 M. At a higher concentration, the effect starts to diminish because of the nearly saturated adsorption of OH_{ad}^- at the total active sites.

The CVs at various scan rates were performed between 0.8 and 1.0 V as shown in Figure S2 (refer to the Supporting Information). No redox peaks corresponding to Ir can be observed, demonstrating pure EDL-capacitive behavior. EDL capacitance is calculated by a single-point CV current method.[20,51] From Figure 3b, the trend of EDL capacitance with KOH concentration is very similar to that of pseudocapacitance. This observation indicates that these two capacitive processes share similar determinants, that is, OH^- transport from the electrolyte and the available active sites. Both EDL charging and redox reactions take place in IHP, consisted with specially adsorbed OH_{ad}^-. For low KOH concentrations, the high charge transport resistance hinders OH^- transport from the bulk electrolyte to the EDL, leading to an insufficient adsorption of OH_{ad}^-, especially at the less accessible active sites, such as micropores, corners, cracks, and grain boundaries.[49] Moreover, the number of inaccessible sites increases with potential scan rate because of reduced response time. This effect can be identified by the nonlinearity of the EDL current (refer to Figure S2 in the Supporting Information), especially in the conditions of high scan rate and <0.8 M KOH as shown in Figure S3.

In the range of 1.4−1.65 V, the integrated area of LSV shown in Figure 3c indicates that the OER activity of IrO_x in 4 M KOH is around 6.5 times higher than that in 0.1 M KOH. The catalytic overpotential at 10 mA cm^{-2} decreases by 86 mV when changing KOH from 0.1 to 4.0 M. The electrolyte-dependent performance is further analyzed by *IR*-corrected Tafel plots (refer to Figure S4 in the Supporting Information). Two distinct Tafel regions can be observed at around 1 and 10 mA cm^{-2}, which is a common feature of the OER Tafel plots as presented in the literature.[3,20,52] The change of Tafel slopes implies a shift of either the rate-determining step (RDS) within a given pathway or the adsorption potential of the reaction intermediates.[3,53] Figure 3d shows that the IrO_x catalyst in the concentrated KOH (>0.8 M) has a lower and stable Tafel slope, thereby experiencing less kinetic overpotential. The Tafel slope of 0.1 M KOH is close to 70 mV dec^{-1} at 1 mA cm^{-2}, indicating that the RDS of OER is the OH^- adsorption (i.e., $*OH_{ad} + OH_{ad}^- \leftrightarrow *O_{ad}^- + H_2O$).[3] When increasing the KOH concentration, the OH^- transport from the bulk electrolyte solution becomes more facile and the Tafel slope is gradually reduced to 50 mV dec^{-1}. The reduction of Tafel slope implies that the RDS shifts toward the second electron-transfer step ($*O^- \rightarrow *O + e^-$), which in turn improves the reaction kinetics. At a higher OER current density, that is, 10 mA cm^{-2}, an apparent increase of Tafel slope can be observed in a lower concentration region (<0.8 M). This may be resulted from the charge transport limitations caused by high ionic transport resistance in bulk electrolyte and active site blocking due to generated O_2 coverage, both of which can be significantly improved by increasing electrolyte concentration. These improvements can be ascribed to the facial OH^- adsorption in IHP, which primarily reflects the impact of the inner-sphere electron transfer mechanism.

The EIS responses during OER are reported in Figure 3e. The applied dc potential (i.e., 1.55 V) is in the mixed kinetics diffusion region. On the basis of a two-time constant processes, the equivalent circuit LR_Ω (R_{ct} CPE_1) (R_1 CPE_2) is used to simulate EIS results.[54,55] These circuit elements L, R_Ω, R_{ct}, R_1, and CPE symbolize inductor, Ohmic resistance, charge-transfer resistance, intermediate diffusion/adsorption resistance, and constant phase element, respectively.[20] The CPE is incorporated into this model to represent nonideal capacitance because of heterogeneity, porous surface, and EDL reconstruction.[56,57] The fitted parameters are given in Table S2. Using our newly developed method, the electrochemical surface area (ECSA) can be calculated from EIS spectra with high accuracy.[20] As shown in Figure 3f, Ohmic resistance (R_Ω), total polarization resistance (R_{ct} + R_1), and ECSA exhibit similar dependence on KOH concentration. This finding indicates that all these key parameters have a significant influence on OER performance. A sharp change can be

DOI: 10.1021/acsami.9b06889
ACS Appl. Mater. Interfaces XXXX, XXX, XXX−XXX

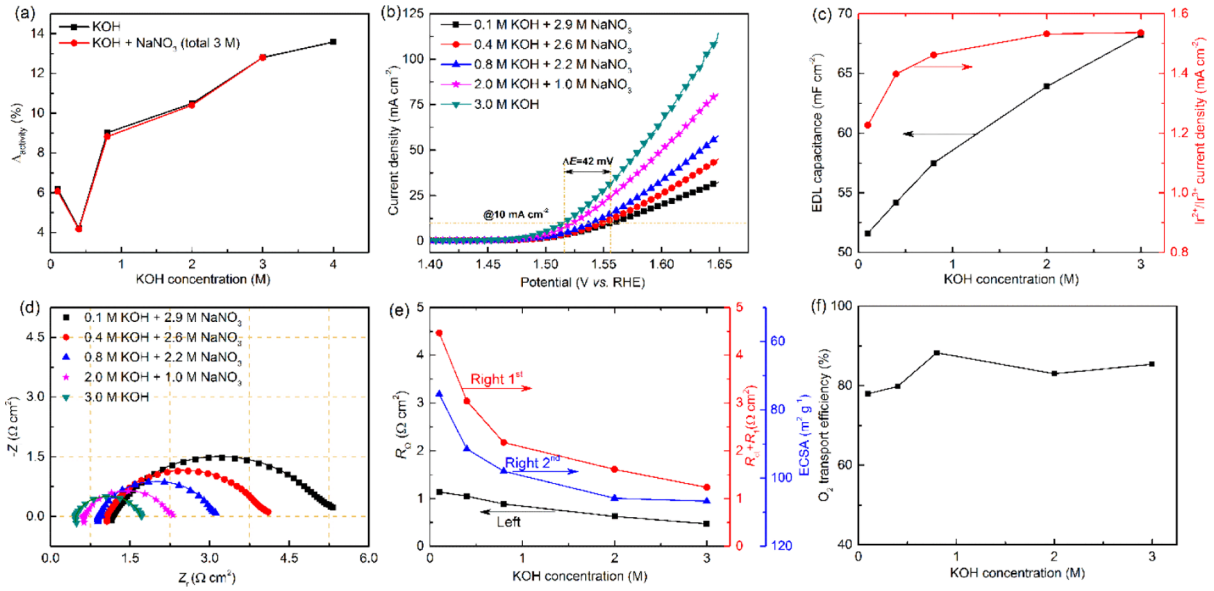

Figure 5. Effects of KOH−$NaNO_3$ on electrocatalytic OER. (a) Activity degradation after 10 000 cycles; (b) LSV curves at 2 mV s^{-1}; (c) EDL capacitance and pseudocapacitive current density; (d) EIS spectra at 1.55 V, symbols—raw data; lines—linear fit to the data; (e) simulated R_Ω, R_{ct} + R_1, and ECSA; and (f) O_2 transport efficiency at 0.5 mA of disk current as a function of KOH concentration.

observed in the concentration range of 0.1−0.8 M, followed by a much gentler change for further increased KOH concentration. This trend is consistent with that of EDL capacitance, pseudocapacitance, and Tafel slopes, demonstrating the crucial roles of inner-sphere OH_{ad}^- in electrocatalytic OER.

As illustrated in Figure 4a, the TF-RRDE setup was employed to study interfacial O_2 transport efficiency (ε_{O_2}) during OER. The Pt-ring potential was held at 0.4 V for the oxygen reduction reaction (ORR). Unlike traditional LSV, the potential sweep in the SCV measurement is a series of staircase steps and the current is recorded at the disk toward the end of each step. By doing so, the contribution of EDL capacitive current can be minimized. Therefore, ε_{O_2} can be calculated as

$$\varepsilon_{O_2} = \frac{i_d - |i_r|/N}{i_d} \times 100\% \quad (2)$$

where i_d and i_r are the measured disk and ring currents, respectively. The RRDE collection efficiency (N) is 37.4% based on our previous work.[20]

The ORR current at the ring electrode increases with increasing oxygen evolution current as observed at the disk shown in Figure 4b. As shown in Figure 4c, ε_{O_2} calculated at 0.5 mA disk current increases from 48.1 to 84.3% with KOH concentration, indicating the enhancement of O_2 transport in EDL. When the disk current is further increased, the ring approaches the limiting current because of maximum O_2 coverage at the disk surface. Moreover, the ring-limiting current decreases with increasing KOH concentration, which further confirms the improvement of interfacial O_2 transport.

3.4. Electrocatalytic OER in KOH + $NaNO_3$ Electrolytes. The initial objective of adding $NaNO_3$ to the KOH solution is to reduce the OH^- transport resistant in the bulk electrolyte. To validate the long-term effect of adding $NaNO_3$, stability measurements were conducted by performing CV for 10 000 cycles in O_2 saturation environment. As shown in Figures S5 and S6 (refer to the Supporting Information), the majority of EDL current reduction occurs in the first 500 cycles for all electrolyte samples studied. The overall decay percent of OER activity ($\Delta_{activity}$) is calculated as

$$\Delta_{activity} = \frac{S_1 - S_2}{S_1} \times 100\% \quad (3)$$

where S_1 and S_2 are the integrated LSV area between 1.4 and 1.65 V before and after 10 000 cycle stability tests, respectively. As shown in Figure 5a, no additional degradation effect is caused by Na^+- and/or NO_3^--related behaviors in the EDL, demonstrating that $NaNO_3$ supporting electrolyte is an inert chemical compound for OER on IrO_x. For both series of KOH and KOH + $NaNO_3$ solutions, the minimum degradation can be achieved at 0.4 M KOH concentration, corresponding to the least alkaline corrosion.

As Na^+ and NO_3^- do not directly participate in OER, the experimental results from KOH + $NaNO_3$ electrolytes are expected to establish a clear relationship between OER activity and OH_{ad}^- in IHP. The comprehensive TF-RDE/RRDE results for various KOH + $NaNO_3$ electrolytes are shown in Figure 5b−f, Figures S7−S9, and Table S3 (refer to the Supporting Information). Although each studied $NaNO_3$−KOH electrolyte has the same total ionic concentration (3.0 M), the OER performance in terms of the reaction kinetics, mass transport, and available ECSA still improve with increasing KOH. This implies that facilitating OH_{ad}^- in IHP is an essential factor for alkaline OER. However, compared with the results in KOH electrolyte, the addition of $NaNO_3$ leads to lesser discrepancies in diffusion-controlled Faradaic reactions, such as OER and solid-state redox (Figure 5b,c), whereas the surface-controlled EDL charging behavior exhibits a close to linear relationship with KOH concentration. The decreased discrepancy of the Faradaic behaviors can be attributed to the increase of ionic conductivity with the addition of $NaNO_3$ supporting electrolyte as shown in Figures 2b and 5d,e.

To emphasize the effect of adding $NaNO_3$, the difference ($\Delta = \chi_{KOH+NaNO_3} - \chi_{KOH}$) between the key parameters (χ) for KOH + $NaNO_3$ and the same-concentration KOH is

DOI: 10.1021/acsami.9b06889
ACS Appl. Mater. Interfaces XXXX, XXX, XXX−XXX

Table 1. Summary of Performance Alternations after Adding $NaNO_3$ into KOH Solutions[a]

C_{KOH} (M)	$\Delta_{activity}$ (%)[b]	Tafel slope (mV dec^{-1}) @j_{low}	Tafel slope (mV dec^{-1}) @j_{high}	C_{EDL} (mF cm^{-2})	j_{ps} (mA cm^{-2})	ECSA (m^2 g^{-1})	R_Ω (Ω cm^2)	(R_1 + R_{ct}) (Ω cm^2)	ε_{O_2} (%)
0.1	79.1	−14	−21	−1.1	0.36	18.5	−6.22	−1.41	40
0.4	0.8	−3	−5	−8.8	0.29	13.0	−1.02	0.18	16
0.8	−23.8	4	7	−6.5	0.25	9.9	−0.23	0.60	14
2.0	−8.6	2	4	−1.9	0.15	6.7	0.06	0.06	7

[a]The total cation/anion concentration is 3 M in the $NaNO_3$-containing KOH solution. [b]$\Delta_{activity}$ is calculated by eq 3 in the range of 1.4−1.65 V. "−" indicates the activity loss.

calculated and summarized in Table 1. On the basis of the new results of $\Delta_{activity}$ and Tafel slopes, the charge transport in the aqueous electrolyte and interfacial O_2 removal have a dominant effect on OER for the 0.1 and 0.4 M KOH electrolytes. However, further increasing the KOH concentration (to 2.0 M) results in smaller differences in C_{EDL}, R_Ω, ε_{O_2}, and ECSA between the electrolytes with and without $NaNO_3$. In this context, the OER activity starts to decrease after introducing $NaNO_3$, which indicates that the outer-sphere Na_{ad}^+ adsorption may be important for interfacial OH_{ad}^- activity.

When adding $NaNO_3$, the excessive amount of the negative OH_{ad}^- in the compact Helmholtz planes tends to repel the inert NO_3^- anion. According to the investigation of 1 M KOH + x M $RbNO_3$ (x = 0, 0.1, 1.0, and 2.0) as shown in Figure S10 (see the Supporting Information), the NO_3^- ions are found to have less effect on OH^- activity, accessible active sites, and thereby OER performance. On the other hand, the nature of this interaction between M_{ad}^+ and OH_{ad}^- has been proposed as a form of noncovalent bond.[17] As illustrated in Figure 1, the cation can interact directly with OH_{ad}^- in IHP, which can be considered as a blockage/poison of active sites. In the presence of Na^+, the adsorbed OH_{ad}^- serves as an anchoring point for the hydrated cations through noncovalent ionic bonding, leading to the formation of $(H_2O)_xNa_{ad}^+\square\square\square OH_{ad}^-$ clusters. In this case, the adsorbed OH^- in IHP has a direct interaction with nonspecially adsorbed Na^+ in OHP. This noncovalent bonding can influence the rate-limiting OH_{ad}^- mobility and thereby increase the Faradaic reaction energy barrier as observed in the mixed electrolyte with ≥0.8 M KOH. The proposed noncovalent bonding between Na_{ad}^+ and OH_{ad}^- is supported by the alternations of cluster size (Figure 2a), electrolyte pH (Figure 2c), and C_{EDL}. Unlike Na^+, the K^+ cation with a larger ionic size might form $(H_2O)_{x-1}K_{ad}^+\square\square\square H_2O\square\square\square OH_{ad}^-$ clusters because of its weak interaction with OH_{ad}^-, corresponding to the hydrogen bonding formed between hydrated water and OH_{ad}^-. There exists an additional water bilayer between K_{ad}^+ cations and OH_{ad}^- groups, resulting in a decrease of cation−OH_{ad}^- interaction energy in a sense. In this situation, K^+ has a minimal effect on OER Faradaic reaction because of this additional H_2O buffer layer. Moreover, the oxygenated OER intermediates, such as O_{ad}, OH_{ad}, and OOH_{ad}, may have similar interactions with nonspecially adsorbed cations. Therefore, the strength of these interfacial interactions through a noncovalent bond can influence the EDL structure and the electrocatalytic activity of OER. On the basis of our understanding, a model of the ionic interactions shown in Figure 6a is proposed to illustrate the above observations.

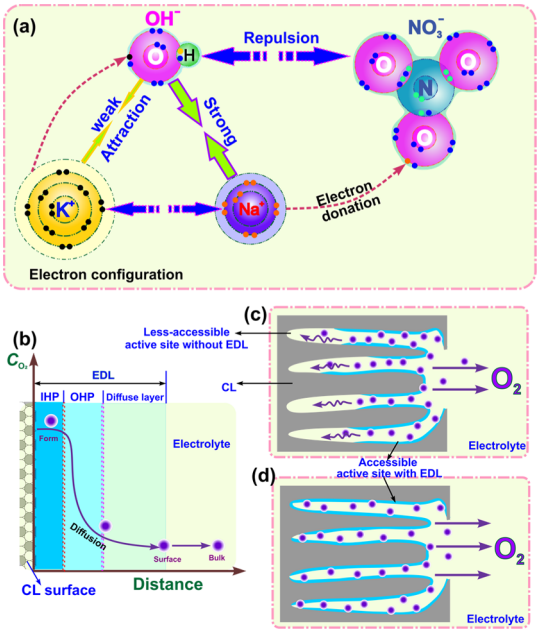

Figure 6. Schematic illustration of (a) ionic interactions and (b) oxygen transport from the reaction interface to the bulk electrolyte solution and interfacial oxygen diffusion in the electrolyte solution with (c) low and (d) high ionic conductivity.

More evidence for the proposed model can be observed from pseudocapacitive current density (j_{ps}) and ECSA (from EIS at 1.55 V), both show the same dependency on KOH concentration in Table 1. From the perspective of reaction mechanism, both solid-state redox and OER occur at available interfacial sites and have similar characteristics.[46,48,58] These two Faradaic reactions strongly depend on the applied potential and mass transport.[58] The charge transport resistance decreases because of the addition of $NaNO_3$, which results in an increase of j_{ps} and ECSA. In addition, the interfacial O_2 transport efficiency also increases with the addition of $NaNO_3$. Conversely, EDL capacitance (C_{EDL}), calculated from CV results, decreases when adding $NaNO_3$. This suggests that C_{EDL} is not proportional to the available active surface area and therefore is not a reliable indicator for OER performance. An important variable is the nonspecially adsorbed Na_{ad}^+, which decreases OH_{ad}^- mobility in EDL. These observations confirm that the interfacial pseudocapacitive behavior is more reliable for measuring the accessible active sites toward OER than EDL charging capacitive process observed by the traditional CV method.[43,51]

Another new finding is related to the interfacial O_2 transport, which is a crucial process for efficient OER. The generated O_2 molecules can be dissolved and adsorbed on the catalyst

DOI: 10.1021/acsami.9b06889
ACS Appl. Mater. Interfaces XXXX, XXX, XXX−XXX

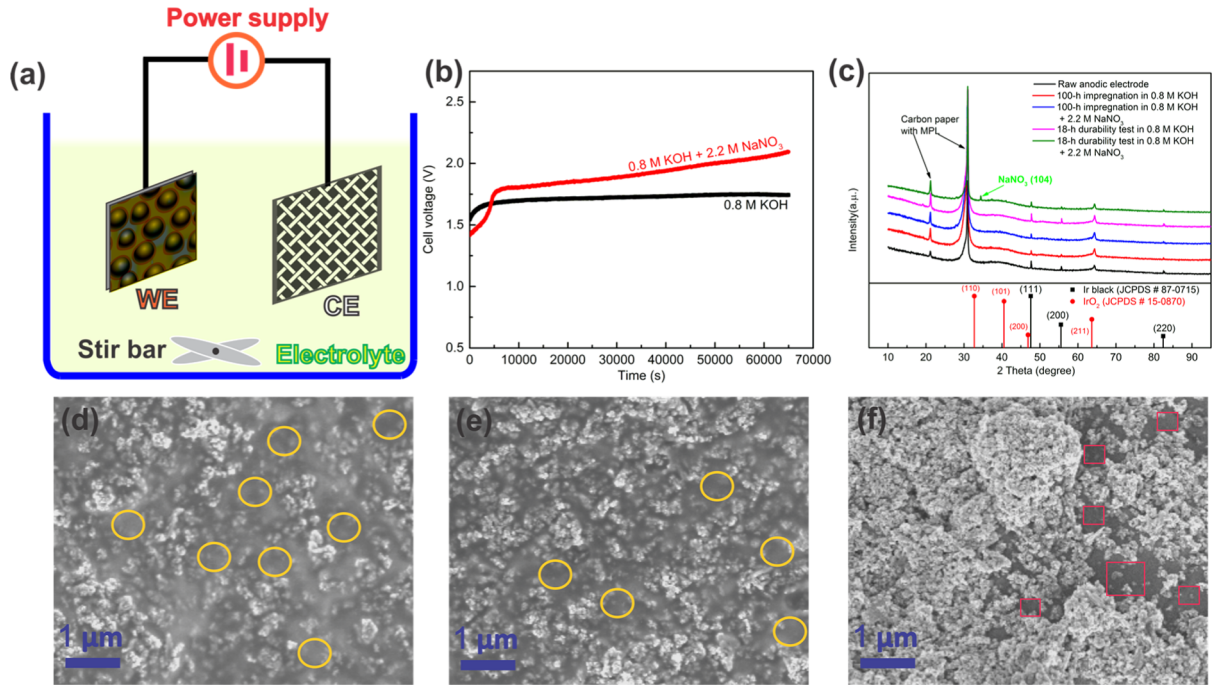

Figure 7. Electrolyte effects in an alkaline electrolyzer. (a) Experimental setup for durability tests. (b) Voltage degradation of durability test at a constant current density of 50 mA cm^{-2}. (c) XRD patterns of IrO_x–Nafion catalyst layer loaded on carbon fiber paper with an MPL. (d–f) SEM images of IrO_x–Nafion ionomer catalyst layers before durability test and after 18 h of durability test in 0.8 M KOH and 0.8 M KOH + 2.2 M $NaNO_3$, respectively. Yellow circles in (d,e) indicate ionomer clusters, while the red squares in (f) confirm catalyst–Nafion losses.

surface by strong van der Waals forces. In this case, the O_2 molecules would block the OH_{ad}^- ions from reaching the active surface, thus slowing down the charge-transfer process. The O_2 transport efficiency (ε_{O_2}) in different KOH–$NaNO_3$ electrolytes with the same ionic concentration is relatively constant as shown in Figure 5f. In contrast, Figure 4c shows that ε_{O_2} increases significantly with KOH concentration. This indicates that interfacial O_2 transport has a dependence on the electrolyte solution. As illustrated in Figure 6b, the bulk of the generated O_2 molecules are transported from the EDL to the bulk electrolyte through convective diffusion process as designed by the TF-RRDE experiment.

The reported ε_{O_2} was calculated at 0.5 mA in all studied electrolyte solutions, which ensures the same oxygen generation at a current well below the limiting current. This indicates that the O_2 concentration in the EDL is lower than the critical concentration, where the maximum gas coverage is achieved at the reaction interface. In this context, we hypothesize a relationship between the O_2 diffusion and the ionic conductivity of the electrolyte solution as illustrated in Figure 6c,d. In the low-concentration KOH, the less accessible sites are not actively participating in OER and can trap the generated O_2. These less accessible sites can exist in micropores, corners, cracks, grain boundaries, and so forth. In the case of high ionic conductivity electrolyte, the improvement of the interfacial O_2 transport can be ascribed to the increasing utilization of the less accessible active sites as indicated in Figure 6d. Therefore, this newly proposed electrolyte–O_2 transport relationship implies that the electrocatalytic OER can be facilitated by enhancing the ionic conductivity of the reaction interface.

3.5. Electrocatalytic OER in a Liquid Alkaline Electrolyzer. As illustrated in Figure 7a, an aqueous electrolyzer system was designed to study the electrolyte effect on OER activity and durability. The GDE with 3 mg cm^{-2} loading of IrO_x was used as the OER electrode. As shown in Figure 7b, increased voltage degradation was observed with the addition of 2.2 M $NaNO_3$ into 0.8 M KOH. From 1.5 to 18 h of continuous operation at 50 mA cm^{-2}, the cell voltage remained stable in 0.8 M KOH but increased more than 300 mV in 0.8 M KOH + 2.2 M $NaNO_3$. The XRD patterns shown in Figure S11 (refer to the Supporting Information) indicate that IrO_x exhibits mostly amorphous state of IrO_2 with narrow peaks of metallic Ir phase. In addition, the IrO_x catalyst and the gas diffusion layer did not show any significant change after the 18 h durability test or the 100 h impregnation in both electrolytes as shown in Figure 7c. However, an additional peak at around 34.3° was observed from the durability testing sample in 0.8 M KOH + 2.2 M $NaNO_3$. This peak matches well with a hexagonal crystal structure of $NaNO_3$ (JCPDS #36-1474), indicating that the reaction interface formed a strong interplay with $NaNO_3$ during the long-term operation. On the basis of the above TF-RDE observations, the adsorbed Na^+ cations inhibit the movement of reactants/intermediates to the reaction interface, which reduces OER reaction rates.

The SEM images shown in Figures 7d–f and S12 (refer to the Supporting Information) exhibit a severe microstructure change of the durability testing electrode in 0.8 M KOH + 2.2 M $NaNO_3$. These images suggest that the CL suffered from losses of Nafion ionomer and catalyst particles during the continuous OER process, resulting in significant degradation observed in Figure 7a. The SEM images also reveal an important interfacial interaction between ionomer and the supporting electrolyte, which requires advance characterization tools for further study.

DOI: 10.1021/acsami.9b06889
ACS Appl. Mater. Interfaces XXXX, XXX, XXX–XXX

4. CONCLUSIONS

In this study, the interfacial interactions between the inner-sphere OH_{ad}^- and outer-sphere M_{ad}^+ have been identified to be a critical factor determining alkaline OER performance. The OER activity of IrO_x increased by around 6.5 times when KOH concentration increased from 0.1 to 4.0 M. Adding $NaNO_3$ serving as the supporting electrolyte to the KOH solution does not influence the long-term stability of IrO_x but significantly changes OER performance. Specifically, the presence of $NaNO_3$ enhances ionic conductivity, O_2 transport, and ECSA. Trends in EDL capacitance and the intrinsic features of the electrolyte, such as hydrodynamic size, ionic conductivity, and pH, show that Na^+ has a stronger covalent interaction with OH^- than K^+ and thus decreases OH_{ad}^- mobility in EDL. Pseudocapacitance from the solid-state redox is found to be more reliable to determine the active sites available for OER than the EDL charging capacitance via the traditional CV method. In addition, increasing ionic conductivity of bulk electrolyte improves the interfacial O_2 transports, which can be ascribed to the increased accessible active sites. Overall, our observations demonstrate that the EDL structure and interfacial interactions are key for electrocatalytic OER.

■ ASSOCIATED CONTENT

Supporting Information

The Supporting Information is available free of charge on the ACS Publications website at DOI: 10.1021/acsami.9b06889.

Additional information on chemical, equipment, ionic properties, and impedance fitting parameters, electrochemical results in either KOH or KOH−$NaNO_3$ electrolyte solutions, XRD pattern of carbon paper with an MPL, and SEM images of IrO_x−Nafion CLs (PDF)

■ AUTHOR INFORMATION

Corresponding Authors

*E-mail: gli27@ucmerced.edu (G.-F.L.).
*E-mail: abel.chuang@ucmerced.edu (P.A.C.).

ORCID

Po-Ya Abel Chuang: 0000-0002-0440-1974

Notes

The authors declare no competing financial interest.

■ ACKNOWLEDGMENTS

The authors would like to thank Professor Ashlie Martini for reviewing our work, Malvern Panalytical for loaning the Zetasizer, and the Imaging and Microscopy Facility at University of California Merced for SEM and XRD measurements. This work is supported by the GREENPower Program (IIID 2015-09) from The Commission on Higher Education—Philippine California Advanced Research Institutes (CHED-PCARI) of the Republic of the Philippines. J. D. Ocon gratefully acknowledges the support from the UP OVPAA Emerging Inter-Disciplinary Research Program (EIDR-C06-003).

■ REFERENCES

(1) Santos, D. M. F.; Sequeira, C. A. C.; Figueiredo, J. L. Hydrogen Production by Alkaline Water Electrolysis. *Quim. Nova* **2013**, *36*, 1176−1193.

(2) Diaz-Morales, O.; Ledezma-Yanez, I.; Koper, M. T. M.; Calle-Vallejo, F. Guidelines for the Rational Design of Ni-Based Double Hydroxide Electrocatalysts for the Oxygen Evolution Reaction. *ACS Catal.* **2015**, *5*, 5380−5387.

(3) Doyle, R. L.; Lyons, M. E. G. The Oxygen Evolution Reaction: Mechanistic Concepts and Catalyst Design. In *Photoelectrochemical Solar Fuel Production: From Basic Principles to Advanced Devices*; Giménez, S., Bisquert, J., Eds.; Springer International Publishing: Cham, 2016; pp 41−104.

(4) Dau, H.; Limberg, C.; Reier, T.; Risch, M.; Roggan, S.; Strasser, P. The Mechanism of Water Oxidation: From Electrolysis via Homogeneous to Biological Catalysis. *ChemCatChem* **2010**, *2*, 724−761.

(5) Jia, Z.; Yin, G.; Zhang, J. 6—Rotating Ring-Disk Electrode Method. In *Rotating Electrode Methods and Oxygen Reduction Electrocatalysts*; Elsevier: Amsterdam, 2014; pp 199−229.

(6) Du, C.; Tan, Q.; Yin, G.; Zhang, J. 5—Rotating Disk Electrode Method. In *Rotating Electrode Methods and Oxygen Reduction Electrocatalysts*; Elsevier: Amsterdam, 2014; pp 171−198.

(7) Shinozaki, K.; Zack, J. W.; Richards, R. M.; Pivovar, B. S.; Kocha, S. S. Oxygen Reduction Reaction Measurements on Platinum Electrocatalysts Utilizing Rotating Disk Electrode Technique. *J. Electrochem. Soc.* **2015**, *162*, F1144−F1158.

(8) Zhong, C.; Deng, Y.; Hu, W.; Qiao, J.; Zhang, L.; Zhang, J. A Review of Electrolyte Materials and Compositions for Electrochemical Supercapacitors. *Chem. Soc. Rev.* **2015**, *44*, 7484−7539.

(9) Colic, V.; Pohl, M. D.; Scieszka, D.; Bandarenka, A. S. Influence of the Electrolyte Composition on the Activity and Selectivity of Electrocatalytic Centers. *Catal. Today* **2016**, *262*, 24−35.

(10) Görlin, M.; Gliech, M.; de Araújo, J. F.; Dresp, A.; Strasser, P.; Strasser, P. Dynamical Changes of a Ni-Fe Oxide Water Splitting Catalyst Investigated at Different pH. *Catal. Today* **2016**, *262*, 65−73.

(11) Giordano, L.; Han, B.; Risch, M.; Hong, W. T.; Rao, R. R.; Stoerzinger, K. A.; Shao-Horn, Y. pH Dependence of OER Activity of Oxides: Current and Future Perspectives. *Catal. Today* **2016**, *262*, 2−10.

(12) Kuo, D.-Y.; Kawasaki, J. K.; Nelson, J. N.; Kloppenburg, J.; Hautier, G.; Shen, K. M.; Schlom, D. G.; Suntivich, J. Influence of Surface Adsorption on the Oxygen Evolution Reaction on IrO2(110). *J. Am. Chem. Soc.* **2017**, *139*, 3473−3479.

(13) Grimaud, A.; Diaz-Morales, O.; Han, B.; Hong, W. T.; Lee, Y.-L.; Giordano, L.; Stoerzinger, K. A.; Koper, M. T. M.; Shao-Horn, Y. Activating Lattice Oxygen Redox Reactions in Metal Oxides to Catalyse Oxygen Evolution. *Nat. Chem.* **2017**, *9*, 457−465.

(14) Cai, W.; Zhao, X.; Liu, C.; Xing, W.; Zhang, J. 2—Electrode Kinetics of Electron-Transfer Reaction and Reactant Transport in Electrolyte Solution. In *Rotating Electrode Methods and Oxygen Reduction Electrocatalysts*; Elsevier: Amsterdam, 2014; pp 33−65.

(15) Suntivich, J.; Perry, E. E.; Gasteiger, H. A.; Shao-Horn, Y. The Influence of the Cation on the Oxygen Reduction and Evolution Activities of Oxide Surfaces in Alkaline Electrolyte. *Electrocatalysis* **2013**, *4*, 49−55.

(16) Lopes, P. P.; Strmcnik, D.; Jirkovsky, J. S.; Connell, J. G.; Stamenkovic, V.; Markovic, N. Double layer effects in electrocatalysis: The oxygen reduction reaction and ethanol oxidation reaction on Au(1 1 1), Pt(1 1 1) and Ir(1 1 1) in alkaline media containing Na and Li cations. *Catal. Today* **2016**, *262*, 41−47.

(17) Strmcnik, D.; Kodama, K.; van der Vliet, D.; Greeley, J.; Stamenkovic, V. R.; Marković, N. M. The Role of Non-Covalent Interactions in Electrocatalytic Fuel-Cell Reactions on Platinum. *Nat. Chem.* **2009**, *1*, 466.

(18) Favaro, M.; Valero-Vidal, C.; Eichhorn, J.; Toma, F. M.; Ross, P. N.; Yano, J.; Liu, Z.; Crumlin, E. J. Elucidating the Alkaline Oxygen Evolution Reaction Mechanism on Platinum. *J. Mater. Chem. A* **2017**, *5*, 11634−11643.

(19) Schmickler, W. Electrode Kinetics for Chemists, Chemical Engineers, and Material Scientists. Von E. Gileadi. VCH Verlagsgesellschaft, Weinheim/VCH Publishers, New York, 1993. 597 S., geb.

DOI: 10.1021/acsami.9b06889
ACS Appl. Mater. Interfaces XXXX, XXX, XXX−XXX

189.00 DM. — ISBN 3-527-89561-2/1-56081-561-2. *Angew. Chem.* **1994**, *106*, 839.
(20) Li, G.; Anderson, L.; Chen, Y.; Pan, M.; Abel Chuang, P.-Y. New Insights into Evaluating Catalyst Activity and Stability for Oxygen Evolution Reactions in Alkaline Media. *Sustainable Energy Fuels* **2018**, *2*, 237−251.
(21) Chakhalian, J.; Millis, A. J.; Rondinelli, J. Whither the Oxide Interface. *Nat. Mater.* **2012**, *11*, 92−94.
(22) Stamenkovic, V. R.; Strmcnik, D.; Lopes, P. P.; Markovic, N. M. Energy and Fuels from Electrochemical Interfaces. *Nat. Mater.* **2017**, *16*, 57−69.
(23) Li, G.; Chuang, P.-Y. A. Identifying the Forefront of Electrocatalytic Oxygen Evolution Reaction: Electronic Double Layer. *Appl. Catal., B* **2018**, *239*, 425−432.
(24) Koper, M. T. M. Theory of Multiple Proton-Electron Transfer Reactions and Its Implications for Electrocatalysis. *Chem. Sci.* **2013**, *4*, 2710−2723.
(25) Bard, A. J.; Faulkner, L. R. *Electrochemical Methods. Fundamentals and Applications*, 2nd ed.; John Wiley & Sons, Inc., 2001.
(26) Bae, J. H.; Han, J.-H.; Chung, T. D. Electrochemistry at Nanoporous Interfaces: New Opportunity for Electrocatalysis. *Phys. Chem. Chem. Phys.* **2012**, *14*, 448−463.
(27) Grimaud, A.; Demortière, A.; Saubanère, M.; Dachraoui, W.; Duchamp, M.; Doublet, M.-L.; Tarascon, J.-M. Activation of surface oxygen sites on an iridium-based model catalyst for the oxygen evolution reaction. *Nat. Energy* **2016**, *2*, 16189.
(28) Franco, D. V.; Da Silva, L. M.; Jardim, W. F.; Boodts, J. F. C. Influence of the Electrolyte Composition on the Kinetics of the Oxygen Evolution Reaction and Ozone Production Processes. *J. Braz. Chem. Soc.* **2006**, *17*, 446−757.
(29) Herranz, J.; Durst, J.; Fabbri, E.; Patru, A.; Cheng, X.; Permyakova, A. A.; Schmidt, T. J. Interfacial Effects on the Catalysis of the Hydrogen Evolution, Oxygen Evolution And Co2-Reduction Reactions for (Co-)Electrolyzer Development. *Nano Energy* **2016**, *29*, 4−28.
(30) Mohammad, A. M.; Awad, M. I.; El-Deab, M. S.; Okajima, T.; Ohsaka, T. Electrocatalysis by nanoparticles: Optimization of the loading level and operating pH for the oxygen evolution at crystallographically oriented manganese oxide nanorods modified electrodes. *Electrochim. Acta* **2008**, *53*, 4351−4358.
(31) Belding, S. R.; Compton, R. G. Cyclic Voltammetry in the Absence of Excess Supporting Electrolyte: The Effect of Analyte Charge. *J. Electroanal. Chem.* **2012**, *683*, 1−13.
(32) Li, G.-F.; Yang, D.; Abel Chuang, P.-Y. Defining Nafion Ionomer Roles for Enhancing Alkaline Oxygen Evolution Electrocatalysis. *ACS Catal.* **2018**, *8*, 11688−11698.
(33) Reier, T.; Nong, H. N.; Teschner, D.; Schlögl, R.; Strasser, P. Electrocatalytic Oxygen Evolution Reaction in Acidic Environments—Reaction Mechanisms and Catalysts. *Adv. Energy Mater.* **2016**, *7*, 1601275.
(34) Kasian, O.; Grote, J.-P.; Geiger, S.; Cherevko, S.; Mayrhofer, K. J. J. The Common Intermediates of Oxygen Evolution and Dissolution Reactions during Water Electrolysis on Iridium. *Angew. Chem., Int. Ed.* **2018**, *57*, 2488−2491.
(35) Suen, N.-T.; Hung, S.-F.; Quan, Q.; Zhang, N.; Xu, Y.-J.; Chen, H. M. Electrocatalysis for the Oxygen Evolution Reaction: Recent Development and Future Perspectives. *Chem. Soc. Rev.* **2017**, *46*, 337−365.
(36) Ramaswamy, N.; Mukerjee, S. Influence of Inner- and Outer-Sphere Electron Transfer Mechanisms during Electrocatalysis of Oxygen Reduction in Alkaline Media. *J. Phys. Chem. C* **2011**, *115*, 18015−18026.
(37) Fawcett, W. R. Fifty years of studies of double layer effects in electrode kinetics-a personal view. *J. Solid State Electrochem.* **2011**, *15*, 1347.
(38) Ramaswamy, N.; Mukerjee, S. Fundamental Mechanistic Understanding of Electrocatalysis of Oxygen Reduction on Pt and Non-Pt Surfaces: Acid versus Alkaline Media. *Adv. Phys. Chem.* **2012**, *2012*, 1.
(39) Tripkovic, D. V.; Strmcnik, D.; van der Vliet, D.; Stamenkovic, V.; Markovic, N. M. The Role of Anions in Surface Electrochemistry. *Faraday Discuss.* **2009**, *140*, 25−40.
(40) Hung, N. G.; Nagy, Z. Kinetics of the Ferrous/Ferric Electrode Reaction in the Absence of Chloride Catalysis. *J. Electrochem. Soc.* **1987**, *134*, 2215−2220.
(41) Kadyk, T.; Bruce, D.; Eikerling, M. How to Enhance Gas Removal from Porous Electrodes? *Sci. Rep.* **2016**, *6*, 38780.
(42) Frydendal, R.; Paoli, E. A.; Knudsen, B. P.; Wickman, B.; Malacrida, P.; Stephens, I. E. L.; Chorkendorff, I. Benchmarking the Stability of Oxygen Evolution Reaction Catalysts: The Importance of Monitoring Mass Losses. *ChemElectroChem* **2014**, *1*, 2075−2081.
(43) McCrory, C. C. L.; Jung, S.; Ferrer, I. M.; Chatman, S. M.; Peters, J. C.; Jaramillo, T. F. Benchmarking Hydrogen Evolving Reaction and Oxygen Evolving Reaction Electrocatalysts for Solar Water Splitting Devices. *J. Am. Chem. Soc.* **2015**, *137*, 4347−4357.
(44) Osgood, H.; Devaguptapu, S. V.; Xu, H.; Cho, J.; Wu, G. Transition Metal (Fe, Co, Ni, And Mn) Oxides for Oxygen Reduction and Evolution Bifunctional Catalysts in Alkaline Media. *Nano Today* **2016**, *11*, 601−625.
(45) Gong, M.; Dai, H. A Mini Review of Nife-Based Materials as Highly Active Oxygen Evolution Reaction Electrocatalysts. *Nano Res.* **2015**, *8*, 23−39.
(46) Liu, W.-J.; Hu, X.; Li, H.-C.; Yu, H.-Q. Pseudocapacitive Ni-Co-Fe Hydroxides/N-Doped Carbon Nanoplates-Based Electrocatalyst for Efficient Oxygen Evolution. *Small* **2018**, *14*, 1801878.
(47) Béguin, F.; Raymundo-Piñero, E.; Frackowiak, E. Electrical Double-Layer Capacitors and Pseudocapacitors. *Carbons for Electrochemical Energy Storage and Conversion Systems*; CRC Press, 2009; pp 329−375.
(48) Eftekhari, A. From Pseudocapacitive Redox to Intermediary Adsorption in Oxygen Evolution Reaction. *Mater. Today Chem.* **2017**, *4*, 117−132.
(49) Ardizzone, S.; Fregonara, G.; Trasatti, S. Inner and Outer Active Surface of RuO_2 Electrodes. *Electrochim. Acta* **1990**, *35*, 263−267.
(50) Jung, S.; McCrory, C. C. L.; Ferrer, I. M.; Peters, J. C.; Jaramillo, T. F. Benchmarking Nanoparticulate Metal Oxide Electrocatalysts for the Alkaline Water Oxidation Reaction. *J. Mater. Chem. A* **2016**, *4*, 3068−3076.
(51) McCrory, C. C. L.; Jung, S.; Peters, J. C.; Jaramillo, T. F. Benchmarking Heterogeneous Electrocatalysts for the Oxygen Evolution Reaction. *J. Am. Chem. Soc.* **2013**, *135*, 16977−16987.
(52) Doyle, R. L.; Lyons, M. E. G. Kinetics and Mechanistic Aspects of the Oxygen Evolution Reaction at Hydrous Iron Oxide Films in Base. *J. Electrochem. Soc.* **2013**, *160*, H142−H154.
(53) Shinagawa, T.; Garcia-Esparza, A. T.; Takanabe, K. Insight on Tafel Slopes from a Microkinetic Analysis of Aqueous Electrocatalysis for Energy Conversion. *Sci. Rep.* **2015**, *5*, 13801.
(54) He, C.; Tao, J. Three-dimensional hollow porous Co 6 Mo 6 C nanoframe as an highly active and durable electrocatalyst for water splitting. *J. Catal.* **2017**, *347*, 63−71.
(55) Li, H.; Chen, Z.; Yu, Q.; Zhu, W.; Cui, W. Effects of Tungsten Carbide on the Electrocatalytic Activity of PbO2-WC Composite Inert Anodes during Zinc Electrowinning. *J. Electrochem. Soc.* **2017**, *164*, H1064−H1071.
(56) Costa, F. R.; Franco, D. V.; Da Silva, L. M. Electrochemical Impedance Spectroscopy Study of the Oxygen Evolution Reaction on a Gas-Evolving Anode Composed of Lead Dioxide Microfibers. *Electrochim. Acta* **2013**, *90*, 332−343.
(57) Orazem, M. E.; Frateur, I.; Tribollet, B.; Vivier, V.; Marcelin, S.; Pébère, N.; Bunge, A. L.; White, E. A.; Riemer, D. P.; Musiani, M. Dielectric Properties of Materials Showing Constant-Phase-Element (CPE) Impedance Response. *J. Electrochem. Soc.* **2013**, *160*, C215−C225.

DOI: 10.1021/acsami.9b06889
ACS Appl. Mater. Interfaces XXXX, XXX, XXX−XXX

(58) Eftekhari, A.; Mohamedi, M. Tailoring Pseudocapacitive Materials from a Mechanistic Perspective. *Mater. Today Energy* **2017**, *6*, 211−229.

DOI: 10.1021/acsami.9b06889
ACS Appl. Mater. Interfaces XXXX, XXX, XXX−XXX